7798 *Biochemistry* **2010,** *49,* 7798–7810
DOI: 10.1021/bi101064w

BIOCHEMISTRY
including biophysical chemistry & molecular biology
Article

Visualizing the Metal-Binding Versatility of Copper Trafficking Sites[†,‡]

Adriana Badarau,[§] Susan J. Firbank,[§] Andrew A. McCarthy,[∥] Mark J. Banfield,[⊥] and Christopher Dennison*[,§]

[§]*Institute for Cell and Molecular Biosciences, Medical School, Newcastle University, Newcastle upon Tyne NE2 4HH, U.K.,* [∥]*Grenoble Outstation, European Molecular Biology Laboratory, 6 rue Jules Horowitz, BP181, 38042 Grenoble Cedex 9, France, and* [⊥]*Department of Biological Chemistry, John Innes Centre, Norwich NR4 7UH, U.K.*

Received July 2, 2010; Revised Manuscript Received August 4, 2010

ABSTRACT: Molecular systems have evolved to permit the safe delivery of copper. Despite extensive studies, many copper site structures involved in copper homeostasis, even for the well-studied metallochaperone Atx1, remain unresolved. Cyanobacteria import copper to their thylakoid compartments for use in photosynthesis and respiration and possess an Atx1 that we show can adopt multiple oligomeric states when metalated, capable of binding up to four copper ions. Two-copper- and four-copper-loaded dimers exist in solution at low micromolar concentrations, and head-to-head and side-to-side arrangements, respectively, can be crystallized, with the latter binding a $[Cu_4\{\mu_2\text{-}S^{\gamma}(Cys)\}_4Cl_2]^{2-}$ cluster. The His61Tyr mutation on loop 5 weakens head-to-head dimerization, yet a side-to-side dimer binding a similar cluster as in the wild-type protein, but with phenolate coordination, is present. The cognate metal-binding domains (MBDs) of the P-type ATPases CtaA and PacS, which are proposed to donate copper to and accept copper from Atx1, respectively, are monomeric in the presence of copper. The structure of the MBD of Cu(I)-PacS shows a crystallographic trimer arrangement around a $[Cu_3\{\mu_2\text{-}S^{\gamma}(Cys)\}_3\{S^{\gamma}(Cys)\}_3]^{2-}$ cluster that is very similar to that found for an alternate form of the His61Tyr Atx1 mutant. Copper transfer from the MBD of CtaA to Atx1 is favorable, but delivery from Atx1 to the MBD of PacS is strongly dependent upon the dimeric form of Atx1. A copper-induced switch in Atx1 dimer structure may have a regulatory role with cluster formation helping to buffer copper.

Copper is an essential trace element involved in key processes such as photosynthesis and respiration. The reactivity of copper and its ability to bind at sites for other metals have resulted in the evolution of homeostatic systems for copper (*1*−*10*). Copper pathways typically involve transporters, which allow the metal to cross membranes, and the diffusible cytosolic metallochaperone Atx1 that binds and delivers copper (*1*−*5*, *9*−*12*). Atx1 and the metal-binding domains (MBDs)[1] of copper transporters are structurally related, typically having a ferredoxin-like ($\beta\alpha\beta\beta\alpha\beta$) fold and a MXCXXC metal-binding motif on loop 1/α1 (*9*). This exposed bis-Cys site has a high affinity for Cu(I) (*13*, *14*), preventing oxidation and keeping the metal available for transfer (*15*). It is assumed that Atx1 binds a two-coordinate Cu(I) site via Cys ligands (*2*, *4*, *5*, *9*), but the crystal structure of such a site is not available.

Cyanobacteria, such as *Synechocystis* PCC6803, are rare examples of prokaryotes with a cytoplasmic requirement for copper. The metal is imported for use by plastocyanin and cytochrome oxidase in photosynthetic and respiratory electron transfer, via the P-type ATPases CtaA and PacS, which have been suggested (*11*, *12*) to transport copper across the plasma and thylakoid membranes, respectively (Figure 1). An Atx1 has been shown to interact with the single N-terminal MBDs of the ATPases ($CtaA_N$ and $PacS_N$) and is proposed to shuttle copper between these proteins (*12*). This provides a relatively simple system compared to those in higher organisms such as humans whose two ATPases (ATP7A and ATP7B also known as the Menkes and Wilson disease proteins, respectively) possess six MBDs. Solution structures have been determined for apo-Atx1 (*16*) and apo-$PacS_N$ (*17*) from *Synechocystis*. NMR studies have shown that this Atx1 dimerizes in solution upon Cu(I) binding, and possible copper site structures have been modeled (*16*), with His61 on loop 5 suggested as a ligand (*16*, *18*). In other prokaryotic Atx1s a Tyr is found in this position (also the case in $PacS_N$), while a Lys is present in the eukaryotic proteins and a Phe is normally found in the MBDs (including $CtaA_N$). This residue is in the second coordination sphere and has been suggested to play a role in copper transfer (*17*, *19*−*22*), although mutations in the *Saccharomyces cerevisiae* protein can have a limited effect on *in vivo* activity (*23*). Dimerization upon Cu(I) binding has also been observed for other Atx1s, including the human protein (Hah1) (*24*) and yeast Atx1 (*25*, *26*) and also the Atx1-like CopZ from *Bacillus subtilis* (*27*, *28*), which is part of a copper export system. For CopZ the crystal structure of a dimer possessing a tetranuclear copper cluster and a crystallographic trimer have been

[†]This work was supported by the Biotechnology and Biological Sciences Research Council (BBSRC), Grant BB/E016529. M.J.B. is supported by a Royal Society (United Kingdom) University Research Fellowship.

[‡]The coordinates and structure factors have been deposited in the Protein Data Bank (PDB) with the accession codes 2xmj, 2xmk, 2xmm, 2xmt, 2xmu, 2xmv, and 2xmw.

*To whom correspondence should be addressed. Tel: +44-191-222-7127. Fax: +44-191-222-7424. E-mail: christopher.dennison@ncl.ac.uk.

[1]Abbreviations: MBD, metal-binding domain; WT, wild type; IPTG, isopropyl β-D-thiogalactopyranoside; Tris, tris(hydroxymethyl)aminomethane; SDS−PAGE, sodium dodecyl sulfate−polyacrylamide gel electrophoresis; AAS, atomic absorption spectroscopy; DTT, dithiothreitol; EDTA, ethylenediaminetetraacetic acid; BCS, bathocuproinedisulfonate; Hepes, 4-(2-hydroxyethyl)piperazine-1-ethanesulfonic acid; MS, mass spectrometry; DTNB, 5,5′-dithiobis(2-nitrobenzoic acid); BCA, bicinchoninic acid; Taps, *N*-tris(hydroxymethyl)methyl-3-aminopropanesulfonic acid; rmsd, root-mean-square deviation; LMCT, ligand-to-metal charge transfer.

 Published on Web 08/20/2010

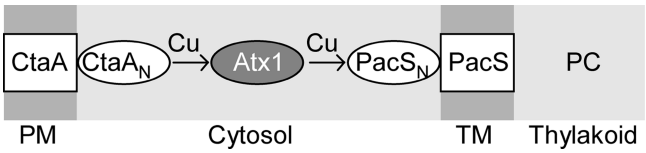

FIGURE 1: The proposed copper-import pathway to the thylakoids of the cyanobacterium *Synechocystis* PCC6803. PM and TM represent the plasma and thylakoid membranes, respectively, and PC represents plastocyanin, the target for copper along with cytochrome oxidase.

found when two- and one-copper-loaded dimers, respectively, are crystallized (*29*, *30*). The crystal structure of a Hah1 dimer formed in the presence of cisplatin in which a single metal ion bridges the two monomers (*31*), similar to the arrangements observed for Cu(I), Hg(II), and Cd(II) Hah1 (*19*), and a yeast Atx1 trimer produced upon treatment with tetrathiomolybdate (*32*) have recently been reported. Scattered data are available suggesting that Atx1 is predisposed to forming higher order structures in the presence of metals.

In this study we show that *Synechocystis* Atx1 can bind up to 2 equiv of copper and can adopt different dimeric arrangements when metalated. A head-to-head dimer is formed in the presence of 1 equiv of copper (Cu^I_1-Atx1) at very low micromolar concentrations. A side-to-side dimer possessing a Cu^I_4 cluster is tighter and exists when 2 equiv of copper are bound (Cu^I_2-Atx1) and binds chloride. His61Tyr Cu^I_2-Atx1 can still form a side-to-side dimer, albeit with an altered copper cluster involving phenolate coordination from the introduced Tyr residue. This mutation removes head-to-head dimerization of the Cu^I_1 form in solution, but the crystal structure reveals a trimer binding a different Cu^I_4 cluster. $CtaA_N$ and $PacS_N$ are monomeric MBDs in the presence of a single Cu(I) ion, and Cu^I_1-$PacS_N$ forms a crystallographic trimer. Copper readily transfers from $CtaA_N$ to Atx1, but the extent of copper transfer to $PacS_N$ is dependent upon the dimeric form of Atx1. A range of structures that an Atx1 can form with its native metal is uncovered with important implications for copper homeostasis.

MATERIALS AND METHODS

Cloning and Site-Directed Mutagenesis. PCR products encoding residues 1−68 and 1−71 of PacS were obtained using pETPAC95 that codes for residues 1−95 [PacS95 (*12*)] as the template. These were subsequently cloned into pET29a, via the *Nde*I and *Eco*RI sites, to give pETPACS68 and pETPACS71 (the latter encoding $PacS_N$). A CtaA fragment encoding residues 26−95 ($CtaA_N$, including a non-native N-terminal Met) was amplified from a plasmid encoding CtaA residues 1−118 (CtaA118). This was also cloned into pET29a via the *Nde*I and *Eco*RI sites giving pETCTAA26-95. The His61Tyr Atx1 variant was generated using QuikChange mutagenesis (Stratagene) with pETATX1 (*12*) as the template using the primers 5′-CGCCTCGGCGGGCTATGAAGTTGAGTGAG-3′ (forward) and 5′-CTCACTCAACTTCATAGCCCGCCGAGGCG-3′ (reverse). Correct sequences for both strands of all DNA constructs were confirmed.

Isolation, Purification, and Reduction of Wild-Type and His61Tyr Atx1. A modified form of a previously reported protocol (*12*) was initially used for the isolation and purification of wild-type (WT) Atx1. *Escherichia coli* BL21(DE3) transformed with pETATX1 was grown in LB media at 37 °C until an OD_{600} of 0.8−1.1 was reached. One millimolar $Cu(NO_3)_2$ was added, and the cells were induced with 1 mM isopropyl β-D-thiogalactopyranoside (IPTG). Cells were harvested after 4 h, resuspended in 25 mM tris(hydroxymethyl)aminomethane (Tris), pH 7.0, sonicated, and centrifuged at 40000*g* for 30 min, and the supernatant was loaded onto a Q-Sepharose FF column (5 mL; GE Healthcare). Proteins were eluted with a linear NaCl gradient (0−1 M) in 25 mM Tris, pH 7.0, with Atx1 eluting around 200 mM NaCl as judged from sodium dodecyl sulfate−polyacrylamide gel electrophoresis (SDS−PAGE) gels. Fractions were combined and concentrated using a stirred ultrafiltration cell (Amicon) with a 3 kDa cutoff membrane. The protein was further purified on a Superdex 75 gel fitration column (16/60; GE Healthcare) equilibrated in 25 mM Tris, pH 7.5, plus 200 mM NaCl and eluted at ~80 mL (purity >95% as judged by SDS−PAGE). Analysis by atomic absorption spectroscopy (AAS) demonstrated that this sample contained ~55% Zn(II)-Atx1 and 45% Cu(I)-Atx1. The previously reported protocol (*12*) for the preparation of reduced apo-Atx1 from a sample purified in this way, which included incubating the protein with 10 mM dithiothreitol (DTT) prior to exposing it to HCl at pH ~2, resulted in the retention of significant amounts of Cu(I) and Zn(II). However, reconstitution with Cu(I) displaced all Zn(II) from the sample, giving homogeneous Cu(I)-loaded Atx1. This indicates that Atx1 has a significantly greater affinity for Cu(I) than Zn(II). Treatment with 20 mM EDTA for 60 min at 4 °C before loading onto the Superdex 75 gel filtration column provided Atx1 fractions eluting at 80.7 mL [dimer containing Cu(I)] and 86.5 mL (monomeric apoprotein). The amount of Cu(I)-Atx1 could be dramatically reduced by not adding $Cu(NO_3)_2$ to the media during induction, resulting in purified protein containing <1% copper and zinc (when treated with EDTA). Monomeric apoprotein from the gel filtration column was fully reduced by an alternative method which involved the addition of 4 mM DTT and incubation overnight. The protein was transferred to an anaerobic chamber and desalted on a PD10 column (GE Healthcare) equilibrated and eluted with 20 mM 4-(2-hydroxyethyl)-piperazine-1-ethanesulfonic acid (Hepes), pH 7.0. The final DTT concentration after this step was less than 2% of the protein concentration. In most cases the protein was passed down a PD10 column at least one more time, ensuring that almost no DTT remained with protein used in subsequent experiments.

For the His61Tyr Atx1 variant, cells were grown as for the WT protein except that $Cu(NO_3)_2$ was omitted. EDTA was used during the purification protocol as the mutant was also isolated with Zn(II) bound. Fully reduced apoprotein was obtained by incubating fractions from the gel filtration column with 4 mM DTT (increasing the DTT concentration did not change the amount of reduced protein, i.e., the A_{280}/[SH] ratio) followed by desalting on a PD10 column, as for the WT protein.

Isolation, Purification, and Reduction of PacS95 and $PacS_N$. PacS95 and $PacS_N$ were isolated and purified using the method described for Atx1 with some modifications. $Cu(NO_3)_2$ was omitted from the media. The cells were resuspended in 25 mM Tris, pH 9.5, and the proteins were eluted from a Q-Sepharose column with a linear 0−1 M NaCl gradient in the same buffer. PacS95 and $PacS_N$ were isolated without zinc or copper. The proteins eluted from the Superdex 75 gel filtration column as monomers at 85.2 mL for PacS95 and 88.3 mL for $PacS_N$ (corresponding to molecular masses of 11.4 and 9.4 kDa, respectively). Fully reduced apo forms were obtained by incubating the protein overnight with 4 mM DTT (increasing the DTT concentration did not change the amount of reduced protein, i.e., the A_{280}/[SH] ratio), transferred to an anaerobic chamber, and desalted on a PD10 column equilibrated and eluted with 20 mM Hepes, pH 7.0.

Isolation, Purification, and Reduction of CtaA118 and $CtaA_N$. CtaA118 was expressed and purified using the same procedure as for PacS95, except that cells were induced (with IPTG) and subsequently grown at 20 °C. The protein proved difficult to purify, and only low yields were obtained. $CtaA_N$, purified using the same method, eluted with Zn(II) from the Superdex 75 gel filtration column in several multimeric forms. When induction was performed in the presence of 1 mM $ZnSO_4$, the protein was found mainly in the insoluble fraction, presumably in inclusion bodies. For all biochemical studies, $CtaA_N$ was purified from inclusion bodies using a fast refolding method (*33*) in which cells from 1 L of culture were harvested, resuspended in 20 mL of 25 mM Tris, pH 7.5, sonicated, and then centrifuged at 40000*g* for 30 min. The pellet was resolubilized by stirring in 25 mM Tris, pH 7.5, plus 6 M urea, 25 mM EDTA, and 10 mM DTT (4 mL) for 2 h at room temperature. This solution was centrifuged at 10000*g* for 15 min, and the supernatant was rapidly added, with stirring, to 200 mL (50-fold dilution) of refolding solution (10 mM Tris, pH 7.5, plus 10 mM DTT and 25 mM EDTA) at 4 °C. The insoluble material was pelleted at 20000*g* for 15 min and the supernatant concentrated using a stirred ultrafiltration cell with a 3 kDa cutoff membrane. The protein was purified on a Superdex 75 gel filtration column, equilibrated in 25 mM Tris, pH 7.5, plus 1 M NaCl. The protein eluted as a single peak at 90.5 mL indicative of the monomeric form. Fractions containing $CtaA_N$ were diluted 10-fold with 25 mM Tris, pH 8.0, (resulting in 0.1 M NaCl) and passed through a Q-Sepharose FF column. The protein did not bind to this column, and the flow-through contained pure $CtaA_N$ with no metals bound. $CtaA_N$ was concentrated to approximately 600 μM using a spinning ultrafiltration device (Vivaspin, 3 kDa cutoff), and fully reduced apo-$CtaA_N$ was prepared using the same method as for $PacS_N$.

Protein Verification and Quantification. All purified proteins were verified by either matrix-assisted laser desorption ionization time-of-flight and/or Fourier transform ion cyclotron resonance mass spectrometry (MS). The concentrations of all fully reduced apoproteins were obtained from the free thiol concentration (two free thiols in WT and His61Tyr Atx1 and three in $PacS_N$ and $CtaA_N$) determined by the reduction of 5,5′-dithiobis(2-nitrobenzoic acid) (DTNB) monitored at 412 nm (ε = 13500 M^{-1} cm^{-1}, calibrated using glutathione) (*34*). The reaction was performed in 100 mM phosphate, pH 8.0, in the presence of 1 mM EDTA and 100 μM DTNB for 10−50 μM free thiols and is fast (< 1 min) for all apoproteins. The DTNB assay was also used to investigate the role of Cys residues in coordinating Cu(I), particularly in WT Atx1 as the presence of metal has a significant effect on this reaction. The protein concentration obtained from DTNB assays for WT Atx1 is in good agreement with that determined from Bradford assays (Coomassie Plus protein assay; Thermo Scientific) using BSA standards and a previously determined correction factor of ∼2.5 (*12*). A similar analysis was performed for the His61Tyr Atx1 mutant, and a smaller correction factor of ∼1.8 was found. Protein concentrations were routinely determined using either the Bradford or bicinchoninic acid (BCA) (BCA protein assay kit; Pierce) assays using the fully reduced apoprotein (either WT or mutant), quantified using DTNB, as standards. Cu(I)-loaded $PacS_N$ and $CtaA_N$ concentrations were determined by Bradford or BCA assays using quantified (DTNB) fully reduced apoprotein as the standards [DTNB assays alone could also be used as the reaction is faster than for Cu(I)-Atx1]. Extinction coefficients at 280 nm (ε_{280}) for His61Tyr Atx1 and $PacS_N$ were determined by denaturing the proteins in 6 M guanidinium chloride in 20 mM sodium phosphate, pH 6.5 (*35*). Values of 1480 and 2350 M^{-1} cm^{-1} were obtained for His61Tyr Atx1 and $PacS_N$, respectively, which are in good agreement with theoretical values of 1280 and 2560 M^{-1} cm^{-1}. An extinction coefficient of 1700 M^{-1} cm^{-1} was determined for $CtaA_N$ (theoretical value of 1280 M^{-1} cm^{-1}) from the absorbance of a fully reduced apo sample, whose concentration was determined from free thiols. These ε_{280} values were used to check protein concentrations obtained with DTNB and protein assays.

Atomic Absorption Spectroscopy. Copper and zinc concentrations were determined by AAS, using an M Series spectrometer (Thermo Electron Corp.) with five standards containing either 0.2 to 1.8 ppm copper in 1.2% HNO_3 or 0.2−1.0 ppm zinc in 1% HCl, using the standard calibration method. Copper concentrations obtained by AAS were routinely checked using the colorimetric ligand BCS by quantification of the $[Cu(BCS)_2]^{3-}$ complex (ε = 12500 M^{-1} cm^{-1} at 483 nm).

Preparation of Cu(I)-Loaded Atx1, $PacS_N$, and $CtaA_N$. Cu(I)-loaded WT Atx1 was prepared in an anaerobic chamber in two ways depending on how reduced apoprotein had been obtained. When the previously reported protocol (*12*) was used to make reduced "metal-free" Atx1, the protein in HCl at pH ∼2 was exposed to a 2-fold molar excess of $[Cu(CH_3CN)_4]PF_6$ (60 mM stock in acetonitrile) under anaerobic conditions prior to the addition of 0.5 M potassium phosphate (pH 7.0) to return the protein solution to pH 7.0. The sample was desalted on a PD10 column equilibrated and eluted with 20 mM Hepes, pH 7.0. The protein contained 2 molar equiv of Cu(I), as determined by AAS, and no Zn(II). Alternatively, apo-Atx1 prepared and reduced (4 mM DTT) at approximately neutral pH was incubated with up to 2 equiv of Cu(I) in 20 mM Hepes, pH 7.0, for 20 min (this procedure was also used for the His61Tyr mutant). WT Cu^I_1-Atx1 was also obtained from Cu^I_2-Atx1 by adding 5 equiv of BCA (for a sample used for crystallography, *vide infra*) and 3 equiv of BCS [for DTNB experiments investigating the effects of Cu(I) binding]. Fully reduced apo-$PacS_N$ and apo-$CtaA_N$ were only loaded with 0−1 Cu(I) equiv, by incubation at pH 7.0, as precipitation occurred when higher amounts of copper were added (*vide infra*). Cu(I)-Atx1 had identical properties regardless of the method of preparation.

Copper and Chloride Titrations. In an anaerobic chamber fully reduced apoprotein (30−130 μM) in 20 mM Hepes, pH 7.0 (pH 8.0 for $CtaA_N$), in either the absence or presence (200 mM) of NaCl was transferred to an anaerobic cuvette (quartz; Hellma). A Cu(I) solution (2.4 mM in 20 mM Hepes, pH 7.0, plus 4% acetonitrile with 200 mM NaCl present when required) was made immediately prior to use from an anaerobically prepared stock solution of $[Cu(CH_3CN)_4]PF_6$ (60 mM in acetonitrile) and titrated using a gastight syringe (Hamilton). Copper concentrations were verified by AAS and also using BCS. UV−vis spectra were acquired on a λ35 spectrophotometer (Perkin-Elmer). Emission spectra were recorded on a Cary Eclipse fluorometer (Varian), either by exciting at 300 nm and following the emission in the 500−700 nm range (emission and excitation slits of 10 nm) or by exciting at 275 nm and following emission at 304 nm (emission slit = 10 nm and excitation slit = 5 nm). The titration of NaCl (2 or 5 M stock) into Cu^I_2-Atx1 (∼60−130 μM) in 20 mM Hepes, pH 7.0, was monitored by UV−vis (in the 200−400 nm range) and by fluorescence emission (500−700 nm upon excitation at 300 nm). The data were fit to eq 1 for WT Cu^I_2-Atx1 to obtain the formation constant β = $[Cu^I_2\text{-Atx1Cl}_2]/([Cu^I_2\text{-Atx1}][Cl^-]^2)$ and to eq 2 for His61Tyr

Cu^I_2-Atx1 to determine the binding constant $K = [Cu^I_2\text{-Atx1Cl}]/([Cu^I_2\text{-Atx1}][Cl^-])$.

$$I = \frac{I_f \beta [Cl^-]^2 + I_0}{\beta [Cl^-]^2 + 1} \quad (1)$$

$$I = \frac{I_f K [Cl^-] + I_0}{K [Cl^-] + 1} \quad (2)$$

In the above equations I_0, I, and I_f represent the intensity of absorbance at 304 nm or emission at 600 nm with no chloride present, at a particular chloride concentration [Cl^-], and at saturating chloride, respectively (derivations of eqs 1 and 2 are given in the Supporting Information). For His61Tyr Atx1 only emission spectra were analyzed as the absorbance around 300 nm is almost unaffected by NaCl. To exclude the influence of ionic strength in these titrations, control experiments were also performed with Na_2SO_4 (with His61Tyr Cu^I_2-Atx1), and no significant increase in luminescence was observed.

Analytical Gel Filtration. Analytical gel filtration was routinely performed using a Superdex 75 GL 10/300 column (GE Healthcare), equilibrated in thoroughly deoxygenated 25 mM Tris, pH 7.5 and 7.0, plus 200 mM NaCl and also in 50 mM phosphate, pH 7.0 (in the presence or absence of 1.5 mM DTT) and at a flow rate of 0.4 mL/min. Experiments were also performed in 25 mM Tris, pH 7.5, plus 700 mM NaCl with and without 4 mM DTT. The column was calibrated using Blue Dextran (2000 kDa), conalbumin (75 kDa), ovalbumin (43 kDa), carbonic anhydrase (29 kDa), ribonuclease A (13.7 kDa), and aprotinin (6.5 kDa) in the same buffer. Cu(I)-loaded proteins typically had an initial concentration of 200−400 μM (in most cases 300 μM, 90 μM for $CtaA_N$ with experiments on WT Cu^I_1-Atx1 and Cu^I_2-Atx1 performed at a range of concentrations). Protein elution was monitored at 280 and 260 nm, and the copper and protein concentrations of all fractions were determined by AAS and DTNB/Bradford assays, respectively. The elution volume of WT Cu^I_1-Atx1 (10−350 μM) loaded onto the column equilibrated in 25 mM Tris plus 200 mM NaCl at pH 7.5 and 7.0 varied with protein concentration. Assuming that the apparent molecular weight of the mixture eluted from the column is a weighted average of the values for monomer and dimer, a dimerization constant (K_{dim}) can be determined using eq 3 (*36*):

$$MW = \frac{M + D\,\dfrac{\sqrt{1 + 8K_{dim}P} - 1}{4}}{1 + \dfrac{\sqrt{1 + 8K_{dim}P} - 1}{4}} \quad (3)$$

in which MW and P are the apparent molecular weight and the total Cu^I_1-Atx1 concentration determined from the chromatograms and M and D are the apparent molecular weights of the monomer and dimer, respectively (eq 3 is derived in the Supporting Information).

Copper(I) Transfer Experiments. Cu(I) transfer was investigated by mixing Cu(I)-loaded protein, i.e., Cu^I_1-Atx1, Cu^I_2-Atx1, Cu^I_1-$PacS_N$, or Cu^I_1-$CtaA_N$, with the apo form of the partner in buffer [20 mM Hepes, pH 7.0, for Atx1-$PacS_N$ transfers and 20 mM *N*-tris(hydroxymethyl)methyl-3-aminopropanesulfonic acid (Taps), pH 8, plus 100 mM NaCl for the Atx1-$CtaA_N$ transfers] for 1.5, 5, or 30 min. After incubation, the mixture was manually loaded onto a Q-Sepharose HP column (1 mL; GE Healthcare). For the Atx1-$PacS_N$ transfers the column was washed successively with 5 mL of buffer, buffer plus 30 mM NaCl, and finally buffer plus 500 mM NaCl. For the Atx1-$CtaA_N$ transfers only two successive washes (5 mL each) of buffer plus 100 mM NaCl and buffer plus 500 mM NaCl were used. One milliliter fractions were collected, and $PacS_N$ and $CtaA_N$ eluted in fractions 2 and 3 of the washes with buffer and buffer plus 100 mM NaCl, respectively, with Atx1 in fractions 1 and 2 of the wash with buffer plus 500 mM NaCl. When copper transfer from Cu^I_2-Atx1 to apo-$PacS_N$ was studied, $PacS_N$ also eluted in fractions 2, 3, and 4 of the buffer wash plus 30 mM NaCl. The fractions containing Atx1, $PacS_N$, and $CtaA_N$ were assayed for copper by AAS and for protein as described above. Control experiments were carried out by loading only one of the partners in the Cu(I) or apo forms onto the Q-Sepharose HP column, and $PacS_N$ eluted in buffer with no salt and also buffer plus 30 mM NaCl, $CtaA_N$ eluted in buffer with 100 mM NaCl, and Atx1 eluted in buffer plus 500 mM NaCl. Exchange equilibrium constants were determined using eqs 4 and 5 for Atx1-$PacS_N$ transfers and eq 6 for $CtaA_N$-Atx1 transfers.

$$K_{ex} = \frac{[Cu^I_1 - PacS_N][apo - Atx1]}{[Cu^I_1 - Atx1][apo - PacS_N]} \quad (4)$$

$$K_{ex} = \frac{[Cu^I_1 - PacS_N][Cu^I_1 - Atx1]}{[Cu^I_2 - Atx1][apo - PacS_N]} \quad (5)$$

$$K_{ex} = \frac{[Cu^I_1 - Atx1][apo - CtaA_N]}{[Cu^I_1 - CtaA_N][apo - Atx1]} \quad (6)$$

Protein Crystallization, Data Collection, Structure Determination, and Refinement. WT apo-Atx1 prepared and reduced at approximately neutral pH was incubated with 1 or 2 molar equiv of Cu(I) in 20 mM Hepes, pH 7.0, to give Cu^I_1-Atx1 or Cu^I_2-Atx1 (method A). WT Cu^I_1-Atx1 was also prepared from Cu^I_2-Atx1 [made by adding Cu(I) to apo-Atx1 in HCl at pH ~2, followed by neutralization (*12*)] by the addition of a 5-fold excess of BCA and desalted on a PD10 column (method B). Samples were concentrated to either 9−10 or 24 mg/mL in 20 mM Hepes, pH 7.0. Diffraction quality crystals were grown under anaerobic conditions at room temperature using the hanging drop method of vapor diffusion in most cases (1.5 μL of protein and well solution). Crystallization and crystal handling regimes that gave rise to data sets for WT Atx1 are shown in Table S1 in the Supporting Information. His61Tyr Cu^I_1-Atx1 was prepared by method A and concentrated to 13−15 mg/mL in 20 mM Hepes, pH 7.0. Diffraction quality crystals of the Cu^I_2 form grew from 25% (w/v) PEG 8000, 200 mM sodium acetate, and 100 mM sodium cacodylate, pH 7.5. Crystals were frozen anaerobically using the well solution supplemented with 5% (w/v) PEG 300 as a cryoprotectant. An alternate crystal form of this variant grew from a screen set up aerobically using a crystallization robot (immediately transferred to the anaerobic chamber and sealed) using the sitting drop method of vapor diffusion (125 nL of protein and well solution) from 2.1 M D,L-malic acid at pH 7.0. Crystals were frozen aerobically in *N*-paratone oil. Crystals of Cu^I_1-$PacS_N$ grew from an 8 mg/mL Cu^I_1-$PacS_N$ sample in 20 mM Hepes, pH 7.0, using 40% (w/v) PEG 300 plus a 100 mM citrate-phosphate mixture, pH 4.6, as the precipitant and were frozen anaerobically in *N*-paratone oil.

All diffraction data were collected at 100 K using synchrotron radiation (ESRF, Grenoble, France, or DLS, Oxford, U.K.) and were processed with MOSFLM/iMOSFLM (*37*) and scaled and

Table 1: Data Collection and Processing Statistics

	WT Atx1 side-to-side dimer			WT Atx1 head-to-head dimer		His61Tyr Atx1		
	aerobic	anaerobic	anaerobic, HR	2 Cu	4 Cu	side-to-side dimer	trimer	$PacS_N$
data collection								
instrumentation	ESRF, 14-2	ESRF, ID29	ESRF, ID23-1	ESRF, ID29	ESRF, ID29/ID23-1	DLS, I03	DLS, I02	DLS, I03
wavelength (Å)	0.933	1.38	0.98	1.38	1.38	1.37	1.38	1.37
space group	*C*2	*C*2	*C*2	*P*1	*P*1	*C*2	$P2_12_12_1$	*P*321
resolution range (Å)[a]	13.81−1.08 (1.14−1.08)	30.02−1.50 (1.58−1.50)	53.22−1.35 (1.42−1.35)	25.00−1.50 (1.58−1.50)	25.57−1.75 (1.84−1.75)	34.06−1.65 (1.74−1.65)	30.00−1.80 (1.90−1.80)	39.47−1.80 (1.90−1.80)
unit cell parameters (Å, deg)	a = 63.43 b = 41.63 c = 55.80 β = 107.71	a = 62.92 b = 41.66 c = 55.74 β = 107.50	a = 62.99 b = 41.71 c = 55.79 β = 107.49	a = 29.09 b = 29.66 c = 38.43 α = 100.89 β = 92.58 γ = 117.91	a = 29.24 b = 29.39 c = 38.70 α = 91.69 β = 101.26 γ = 118.62	a = 62.63 b = 41.40 c = 55.58 β = 106.76	a = 47.64 b = 76.99 c = 90.34	$a = b$ = 45.56 c = 51.83
unique reflections	56359 (7941)	22238 (3218)	29653 (4218)	15929 (2260)	10938 (1593)	16218 (2311)	31381 (4513)	6085 (865)
multiplicity[a,b]	6.4 (6.4)	10.4 (10.3)	4.9 (4.4)	3.8 (3.9)	6.8 (6.9)	5.2 (5.3)	4.8 (4.9)	23.5 (23.9)
[anomalous]		[5.1 (4.9)]		[2.0 (2.0)]	[3.3 (3.4)]	[2.7 (2.7)]	[2.5 (2.6)]	[12.7 (12.6)]
mean $((I)/\sigma(I))$[a,b]	17.9 (4.4)	41.0 (18.2)	15.4 (5.1)	18.2 (3.9)	22.0 (9.7)	14.1 (4.0)	29.7 (13.1)	39.0 (10.3)
completeness (%)[a,b]	95.9 (92.8)	99.6 (99.3)	97.4 (95.9)	90.3 (88.1)	98.4 (97.6)	98.0 (97.0)	99.3 (99.5)	100.0 (100.0)
[anomalous]		[98.9 (97.0)]		[85.5 (85.3)]	[94.0 (93.3)]	[96.2 (95.7)]	[96.0 (96.0)]	[100.0 (100.0)]
R_{merge} (%)[a,b]	5.7 (23.2)	6.0 (16.2)	7.6 (29.2)	5.0 (37.4)	6.0 (29.5)	10.9 (29.4)	10.9 (36.1)	7.4 (42.0)
refinement[c]								
resolution range (Å)[a]	10−1.08	30.02−1.50 (1.54−1.50)	53.22−1.35 (1.39−1.35)	25.00−1.50 (1.54−1.50)	25.57−1.75 (1.80−1.75)	34.06−1.65 (1.69−1.65)	30.00−1.80 (1.90−1.80)	39.47−1.80 (1.85−1.80)
R_{cryst} (%)[a,d]	11.7	15.9 (19.3)	12.9 (14.5)	16.0 (26.3)	26.7 (35.0)	16.5 (23.5)	19.1 (26.3)	24.5 (23.7)
R_{free} (%)[a,d]	14.9	18.5 (19.3)	15.3 (18.9)	20.3 (30.9)	31.2 (36.6)	20.0 (25.0)	25.3 (33.3)	25.9 (28.8)
rms bond (Å)[d]	0.014	0.015	0.013	0.016	0.014	0.012	0.017	0.018
rms angle (deg)[d]	2.1	1.53	1.44	1.49	1.54	1.23	1.47	1.55
no. of non-hydrogen atoms	1248	1222	1173	1040	914	1108	2966	498
ESU (ML) (Å)[d]	0.01	0.04	0.02	0.05	0.15	0.06	0.10	0.07
anisotropic *B*-factors	yes	no	yes	yes	no	no	no	no
Ramachandran outliers	0	0	0	0	1	0	0	0
PDB accession codes	2xmj		2xmk	2xmt	2xmu	2xmm	2xmv	2xmw

[a]Figures in parentheses are those for the highest resolution shell, as given. [b]Reflection statistics are as reported by SCALA (*38*). R_{merge} is calculated as described in SCALA (*38*). [c]Only a part-refined model for the anaerobic WT Atx1 side-to-side dimer, phases used for calculation of anomalous difference map as described. [d]Refinement statistics are as reported by REFMAC5, except for the aerobic Atx1 side-to-side data set which used SHELX.

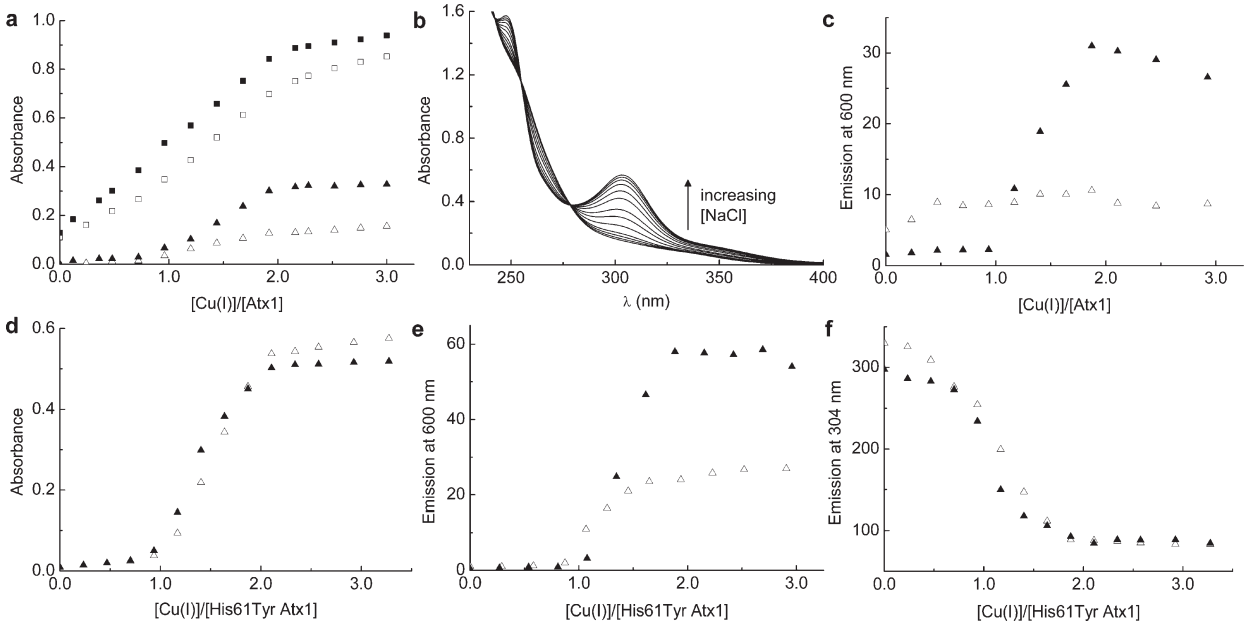

FIGURE 2: Cu(I) binding by Atx1 in 20 mM Hepes at pH 7.0 with open and filled symbols representing data obtained in the absence and presence of NaCl (200 mM), respectively. (a) Plots of absorbance at 250 nm (squares) and 304 nm (triangles) against the [Cu(I)]/[Atx1] ratio ([Atx1] = 50 μM) for WT Atx1. (b) The influence of increasing NaCl concentration (0−136 mM) on the absorption spectrum of WT Cu^{I}_{2}-Atx1 ([Atx1] = 100 μM). (c) A plot of the luminescence at 600 nm against the [Cu(I)]/[Atx1] ratio ([Atx1] = 100 μM) for WT Atx1. Also shown are plots of absorbance at 300 nm (d) and luminescence at 600 nm (e) against the [Cu(I)]/[His61Tyr Atx1] ratio ([His61Tyr Atx1] = 100 μM in (d) and 130 μM in (e)). (f) Quenching of Tyr61 fluorescence upon Cu(I) titration into His61Tyr apo-Atx1 (100 μM).

merged with SCALA [CCP4 suite (*38*)]. Data collection and processing statistics are given in Table 1. The phase set generated by ACORN for the initial WT Atx1 structure was of sufficient quality for automatic building of an essentially complete asymmetric unit by ARP/wARP (*39*). A final model was produced using cycles of model building in COOT (*40*) and refinement with SHELX (*41*). All other structures of Atx1 (WT and His61Tyr) were solved by molecular replacement using either PHASER or MOLREP (CCP4 suite) and a model comprising a monomer of the highest resolution Atx1 side-to-side structure with all ligands removed. Final models were produced using iterative cycles of model building in COOT and refinement, using REFMAC5 (CCP4 suite); anisotropic *B*-factors were refined when appropriate. Anomalous difference maps were calculated from data sets collected near the peak of the copper K-edge and φ_{calc} from a refinement run using the final model excluding the copper atoms. The structure of $PacS_N$ was solved using the single wavelength anomalous dispersion method. A single copper site was located by PHENIX.HYSS (*42*). Phases were calculated and refined using MLPHARE (CCP4 suite) and modified with DM. An initial model was built using ARP/wARP, and cycles of model building (COOT) and refinement (REFMAC5) produced the final model. Anomalous difference maps for copper were calculated as above. Refinement parameters are given in Table 1. MOLPROBITY (*43*) was used to generate Ramachandran plots, and structure superimpositions using LSQMAN (*44*) provided root-mean-square deviations (rmsds) based on C_α atoms. Protein interfaces were analyzed using PISA (*45*), and protein figures have been prepared with PYMOL (DeLano Scientific).

RESULTS

Protein Isolation. The identity of all purified proteins was confirmed by MS, and the experimental and theoretical masses are given in Table S2 in the Supporting Information. The N-terminal region of PacS used previously for two hybrid interactions with Atx1 (*12*) and for solution structure investigations (*17*) consisted of amino acids 1−95 (PacS95, which includes the $\beta\alpha\beta\beta\alpha\beta$ ferredoxin-like domain and the linker to the first transmembrane helix). The NMR structure of PacS95 demonstrates that the C-terminal tail (residues 71−95) is flexible (*17*). Purified PacS95 exhibited multiple bands on a SDS−PAGE gel and several peaks by MS. The largest component corresponded to PacS95 minus the N-terminal Met, with smaller fragments identified as various C-terminal truncations. The two smallest species contained residues 2−68 and 2−71 (both missing Met1). Overexpressed PacS68 was found mainly in the insoluble fraction, whereas PacS71 gave higher levels of mainly soluble protein and has therefore been used as $PacS_N$ in these studies. This protein is stable, shows no signs of C-terminal degradation, and exhibited similar copper-binding properties as PacS95 (*vide infra*). Overexpression of the N-terminal region of CtaA containing residues 1−118 (CtaA118) (*12*) gave low yields of unstable protein, which contained species with several molecular weights. The largest component corresponds to CtaA118 minus Met1, and others involve C- and N-terminal truncations. The smallest species corresponded to Leu26 to His95, and we therefore used CtaA26−95 as the MBD [$CtaA_N$; Met1, Leu2 (Leu26) to His71 (His95), the CXXC is $C^{11}XXC^{14}$, the third Cys is Cys32, and Phe87 which corresponds to His61 of Atx1 and Tyr65 of $PacS_N$ is Phe63]. Apo-$CtaA_N$ is unstable and precipitates at pH 7.0 at concentrations as low as 50 μM. At pH 8.0 the protein is more stable and can be concentrated to about 600 μM providing that a NaCl concentration of 100 mM is maintained.

Cu(I) Binding, Oligomerization States in Solution, and Crystal Structures. Cu(I) binding by WT Atx1 was followed by the appearance of S(Cys) → Cu(I) ligand-to-metal charge transfer (LMCT) transitions in absorption spectra (Figure 2a and Figure S1a,b in the Supporting Information). Surprisingly, these data reveal the sequential binding of two Cys-coordinated Cu(I) ions (see also Figure S1c in the Supporting Information) and the

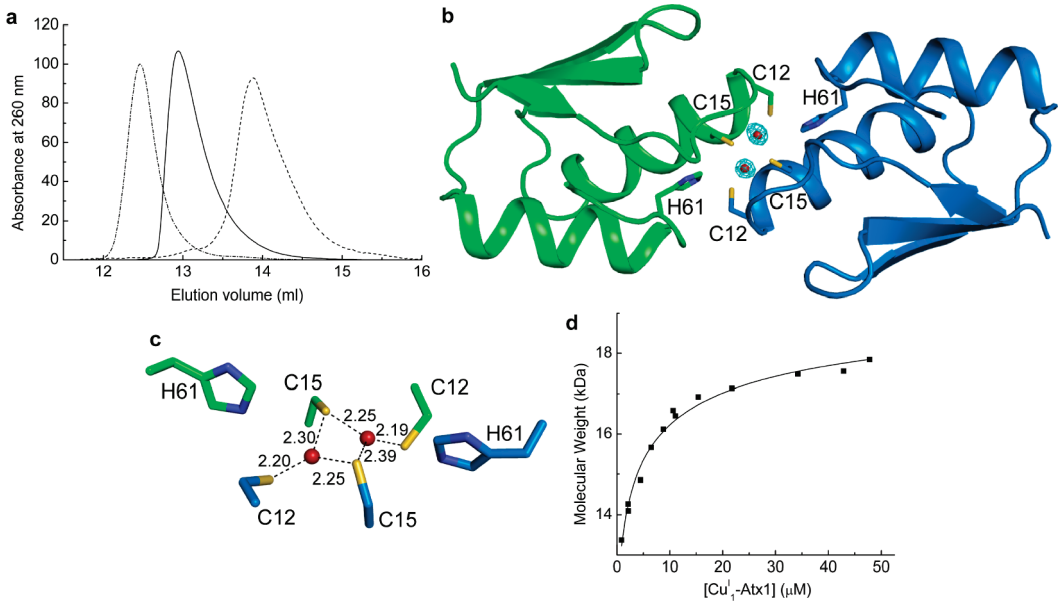

FIGURE 3: Atx1 forms different dimers in the presence of copper and the structure of the head-to-head arrangement. (a) Plots of absorbance at 260 nm (arbitrary units) against elution volume for WT apo- (dashed line), Cu^{I}_{1}-Atx1 (solid line), and Cu^{I}_{2}-Atx1 (dashed and dotted line) from a gel filtration column in 20 mM Tris at pH 7.5 (200 mM NaCl). (b) The WT Cu^{I}_{1}-Atx1 head-to-head dimer with red spheres representing the copper ions, side chains shown as sticks, and the anomalous difference density for copper contoured at 12σ. The copper site structure is shown in detail in (c). (d) The influence of total Cu^{I}_{1}-Atx1 concentration on the calculated molecular weight from the elution volume from the gel filtration column at pH 7.0 (200 mM NaCl) with the line showing a fit of the data to eq 3.

binding of chloride to Cu^{I}_{2}-Atx1 (Figure 2a,b). Cu^{I}_{2}-Atx1 gives rise to Cu(I)-thiolate cluster luminescence at ~600 nm, but only in the presence of chloride (Figure 2c). His61 on loop 5 has been mutated to a Tyr to introduce the residue usually found in this position in prokaryotic Atx1s (and also $PacS_N$). Similar Cu(I) binding characteristics are observed for His61Tyr Atx1 (Figure 2d,e and Figure S1d in the Supporting Information). The presence of chloride has a much smaller influence on the UV−vis spectrum of His61Tyr Atx1 compared to the WT protein (Figure 2d) but still has a significant effect on Cu(I) cluster luminescence for the Cu^{I}_{2} form (Figure 2e). Cu(I) addition quenches Tyr61 fluorescence (Figure 2f), with the second equivalent having the greatest effect.

The dimerization of Atx1 upon Cu(I) binding (*16*) was studied by analytical gel filtration. WT apo-Atx1 is a monomer (*16*) and elutes at a volume corresponding to a molecular mass of 13.2−13.3 kDa (Figure 3a and Table S3 in the Supporting Information) even in the presence of DTT. The Cu^{I}_{1} and Cu^{I}_{2} forms of Atx1 exhibit smaller elution volumes than for the apoprotein, which unexpectedly are different, giving apparent molecular masses of 19.3 and 23.5 kDa, respectively (Figure 3a and Table S3 in the Supporting Information), indicating distinct dimeric forms of the one- and two-copper-loaded proteins. In the presence of 1.5 mM DTT Cu^{I}_{2}-Atx1 elutes as the Cu^{I}_{1}-Atx1 dimer, and the second (weaker) Cu(I) site has been removed (Table S3 in the Supporting Information). UV−vis studies show that this site is also removed by glutathione. The His61Tyr mutation results in monomeric Cu^{I}_{1}-Atx1 and a dimeric Cu^{I}_{2}-species, with a gel filtration elution volume more similar to that for the Cu^{I}_{2} form of the WT protein than the Cu^{I}_{1} dimer (Table S3 in the Supporting Information).

To understand the binding of Cu(I) and chloride by Atx1 and to investigate copper-induced dimerization, we have determined the crystal structures of different forms of the WT protein and also the His61Tyr variant. WT Cu^{I}_{1}-Atx1 crystallizes as a head-to-head dimer (Figure 3b) with a small interface area (~230 Å^2 per monomer). In this complex each of the copper ions is ligated by the S^{γ} atoms of Cys12 and Cys15 from one monomer and Cys15 from the adjacent chain (Figure 3c and Figure S2a in the Supporting Information), with intramolecular S−Cu−S bond angles of approximately 140° (the intermolecular S−Cu−S bond angles range from 93° to 126°). The copper to copper distance is 2.77 Å, and His61 is in the second coordination sphere, hydrogen bonding (via its $N^{\varepsilon 2}$ atom) to Cys15 (S^{γ}) from the same monomer (3.7 Å) and to Cys12 (S^{γ}) from the adjacent chain (3.4 Å). His61 hydrogen bonds via its $N^{\delta 1}$ atom with the $O^{\gamma 1}$ of Thr9 from the same chain. The coordinating S^{γ} atoms accept intramolecular hydrogen bonds from the backbone amides of Ala11 (Cys15) and Ala14 (Cys12), interactions which are present in other Atx1 crystal structures. At protein concentrations below 100 μM the elution volume for WT Cu^{I}_{1}-Atx1 increases with decreasing protein concentration (Figure 3d), indicative of the dimer undergoing dissociation as it passes through the column (*36*). The elution volume, and hence the calculated molecular weight, depends on the average size of the molecules in the population. Appreciable amounts of monomeric Cu^{I}_{1}-Atx1 start to form in the very low micromolar region (Figure 3d), and a stability constant (K_{dim}) for the dimer of $(5 \pm 2) \times 10^5$ M^{-1} [dissociation constant of (2.0 ± 0.8) μM] is obtained at pH 7.5.

A crystal structure of the head-to-head dimer possessing Cu(I) at four sites has been obtained in the absence of chloride (Figure 4) but does not refine well (Table 1), although the positions of the coppers and the ligating residues are unambiguously defined in the electron density (Figure 4a and Figure S2b in the Supporting Information). The head-to-head dimeric arrangement (Figure 4a) is almost unaltered by the presence of the additional copper sites (rmsd for C^{α} atoms of 0.32 Å). The small changes that do occur cannot give rise to the different gel filtration elution volume for Cu^{I}_{2}-Atx1 compared to the Cu^{I}_{1} dimer (Figure 3b), and the Cu(I) cluster in this structure probably forms during crystallization. His61 is involved in coordination at the additional Cu(I) sites in this structure (Figure 4), and the electron density

suggests that these are not fully occupied (Figure 4a and Figure S2b in the Supporting Information). The shortest Cu to Cu distances are ~2.5 Å for the metal ions bridged by Cys12, and the interdomain Cys15 to copper distance is long (~2.9−3.0 Å). The structure of the four copper head-to-head dimer bears some resemblance to that recently published for a *B. subtilis* CopZ dimer with four Cu(I) ions bound, in which metal sites are also partially occupied (*29*). However, the relative orientation of the two monomers is different in these two structures, resulting in altered locations of the metal sites and differences in the clusters.

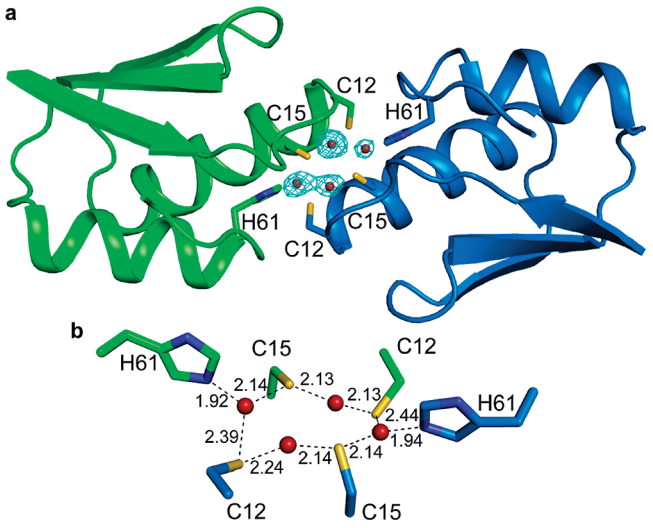

FIGURE 4: Structure of the WT Atx1 head-to-head dimer with four copper ions bound. The copper ions and side chains are depicted as in Figure 3. In (a) the anomalous difference density for copper is shown contoured at 8σ with the copper cluster shown in detail in (b).

Most significantly, whereas the intramonomer Cu(I) site in Atx1 is ~2.9−3.0 Å from Cys15 of the adjacent chain, in CopZ Cys13 (equivalent to Cys12 in Atx1) makes a closer intermonomer approach (2.54 Å) at the corresponding site. Furthermore, the four Cu(I) ions in this Atx1 structure are almost coplanar, which is not the case for the tetranuclear cluster in CopZ.

In the presence of chloride, Cu^{I}_{2}-Atx1 crystallizes as a side-to-side dimer (Figure 5a). The monomers have structures very similar to those found in the head-to-head arrangement (rmsds for C^{α} atoms of 0.7 ± 0.1 Å for the two monomers). Almost identical side-to-side Cu^{I}_{2}-Atx1 dimer structures (rmsd for C^{α} atoms of 0.10 Å) were obtained from the crystallization of Cu^{I}_{1}-Atx1 and Cu^{I}_{2}-Atx1, with the crystal of the former exposed to oxygen for a short period while being frozen. The contact area for the Cu^{I}_{2}-Atx1 side-to-side dimer is larger than for the head-to-head arrangement (~440 $Å^2$ per monomer), and an intermolecular hydrogen bond between Asn25 ($N^{\delta 2}$) and Ala57 (CO) may help to stabilize this complex. This arrangement is similar to the crystallographic Hah1 dimers (*19*, *31*) and also the solution complexes of yeast Atx1 with Ccc2a (*46*) and Hah1 with the first domain of the Menkes ATPase (*47*). The $[Cu_4\{\mu_2\text{-}S^{\gamma}(Cys)\}_4Cl_2]^{2-}$ cluster found at the dimer interface is strikingly symmetrical with all four metal ions in a plane forming a rhombus and Cu to Cu distances of 2.6−3.0 Å (4.7 Å for the long axis of the rhombus) (Figure 5b and Figure S3a in the Supporting Information). The Cu(I) site within each Atx1 monomer is two-coordinate and almost linear (S−Cu−S angle of 166°). At each of the interdomain copper sites the S−Cu−S angles are smaller (153° and 143°), and a distant chloride ligand is present (Figure 5b), with one of these hydrogen bonded by the $N^{\varepsilon 2}$ atoms of His61 from both chains (the $N^{\delta 1}$ atom of His61 hydrogen bonds with the $O^{\gamma 1}$ of Thr9). The Cu−S bond lengths for the interdomain sites are similar to those at the intramolecular copper sites, and the

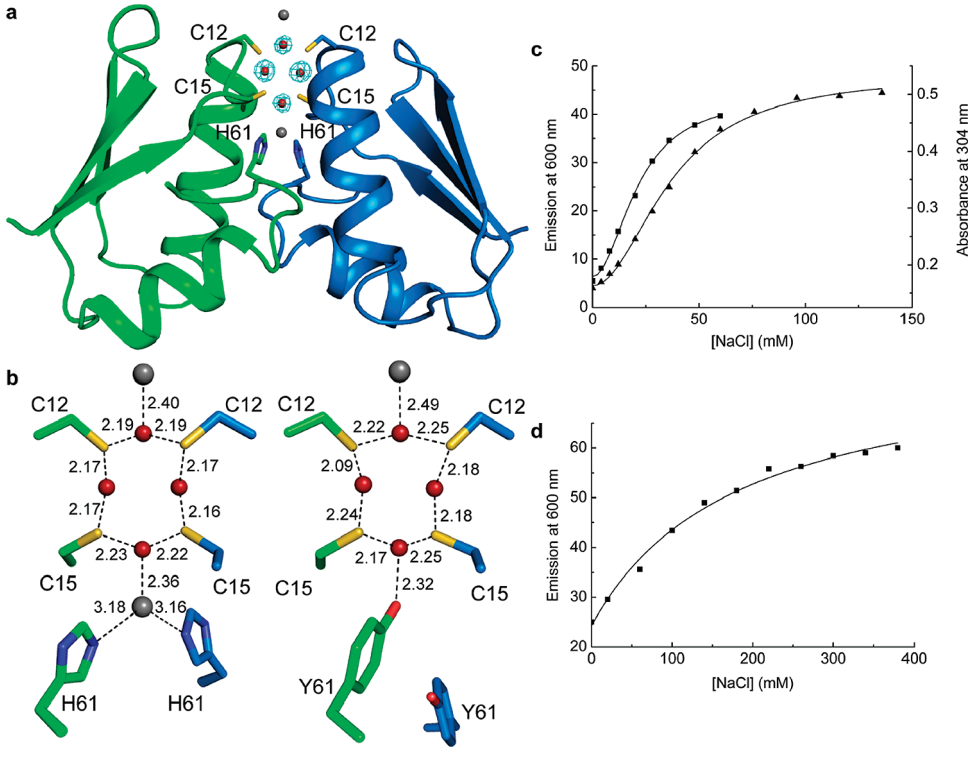

FIGURE 5: Cu^{I}_{2}-Atx1 forms an alternate dimer. (a) The Cu^{I}_{2}-Atx1 side-to-side dimer with the copper ions and side chains depicted as in Figure 3, chloride ions as gray spheres, and the anomalous difference density for copper contoured at 12σ. (b) The $[Cu_4\{\mu^2\text{-}S^{\gamma}(Cys)\}_4]$ clusters found in the WT (left) and His61Tyr (right) Cu^{I}_{2}-Atx1 side-to-side dimers. (c) The influence of NaCl concentration on the absorbance at 304 nm (triangles) and the luminescence at 600 nm (squares) for WT Cu^{I}_{2}-Atx1 (100 μM) in 20 mM Hepes, pH 7.0. (d) The influence of NaCl concentration on the luminescence at 600 nm for His61Tyr Cu^{I}_{2}-Atx1 (130 μM) in 20 mM Hepes, pH 7.0. The fits shown are explained in the text.

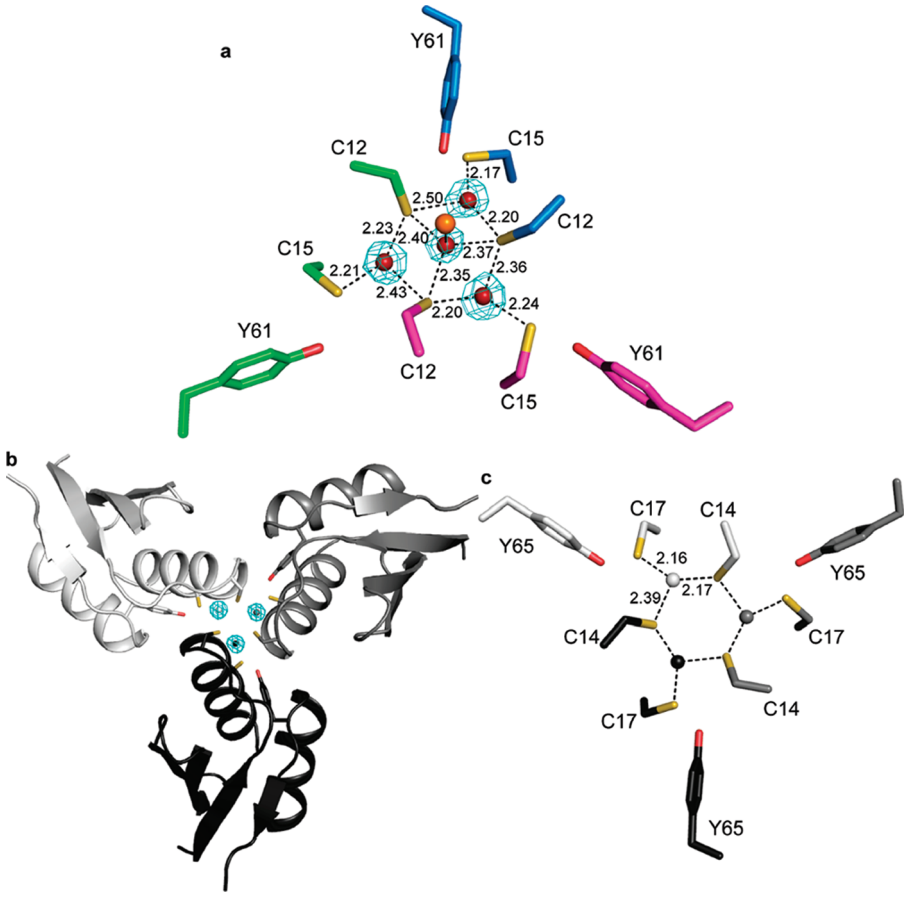

FIGURE 6: The copper cluster in the His61Tyr Atx1 trimer and the structure of the Cu^{I}_{1}-$PacS_N$ trimer. (a) Structure of the $[Cu_4\{\mu_3\text{-}S^{\gamma}(Cys)\}_3\{S^{\gamma}(Cys)\}_3(H_2O)]^{2-}$ cluster in the His61Tyr Atx1 variant with the copper ions and side chains depicted as in Figure 3, the oxygen atom shown as an orange sphere, and the anomalous difference density for copper contoured at 5σ. The Cu−O bond length is 2.23 Å, and the distances from the water-bound copper to the other three copper ions are 2.49, 2.59, and 2.65 Å. (b) The crystallographic $PacS_N$ trimer with the monomers, associated side chains and copper ions in different shades of gray. Also included is the anomalous difference density contoured at 15σ. The arrangement of the copper sites in the $PacS_N$ trimer is shown in (c). The intramolecular S−Cu−S bond angle is 141° while the intermolecular S−Cu−S bond angles are 102° and 117°.

chloride ions are probably not essential for cluster formation. The S^{γ} atoms of the Cys ligands accept hydrogen bonds from the backbone amides of Ala14 and Ala11, respectively, as in the head-to-head arrangement.

The titration of NaCl into WT Cu^{I}_{2}-Atx1 monitored by both absorbance at 304 nm and emission at 600 nm does not fit well to a one chloride binding site model. Much better fits (Figure 5c) are obtained using a model (eq 1) in which two Cl^- ions are assumed to bind simultaneously to the Cu^{I}_{2}-Atx1 dimer. These give rise to apparent formation constants (β) of $(2.2 \pm 0.2) \times 10^3$ M^{-2} and $(7.2 \pm 0.8) \times 10^2$ M^{-2} from the fluorescence and UV−vis titrations, respectively (the discrepancy between the β values may be because the model assumes that no monochloro intermediate forms and that the final absorbance or emission is due to the dichloro species). This is consistent with two sites for chloride as found in the Cu^{I}_{2}-Atx1 side-to-side dimer crystal structure (Figure 5a,b). Both data sets were also simultaneously fit to a model that includes the presence of two monochloro intermediates. In this model chloride binding at the external site gives rise to an increase in fluorescence (as seen for His61Tyr Atx1, *vide infra*), while chloride binding at the internal site is responsible for the increase in absorbance. The fit was unsuccessful for sequential Cl^- binding, i.e., when $K_1 > K_2$, and required cooperative binding, i.e., $K_1 < K_2$, where K_1 and K_2 are the binding constants of the first and second chloride, respectively, to the Cu^{I}_{2}-Atx1 dimer. The β value obtained from the simultaneous fit is $(1.03 \pm 0.2) \times 10^3$ M^{-2}, intermediate between the values found from individual fits. A binding constant of (15.9 ± 1.7) M^{-1} was found for Cl^- association at the external site.

The gel filtration elution volume of Cu^{I}_{2}-Atx1 was also found to depend on protein concentration. At 4 μM, this form elutes at a calculated molecular mass of 19.0 kDa (compared to 23.5 kDa at 60 μM), which indicates a dimerization constant of approximately 10^6 M^{-1} (eq 1, M = 13.2 kDa and D = 23.5 kDa). However, the protein eluted as a mixture of Cu^{I}_{2}-Atx1 and Cu^{I}_{1}-Atx1, indicating that following dimer dissociation the weaker copper is lost on the gel filtration column. Therefore, a lower limit for K_{dim} of approximately 10^6 M^{-1} (dissociation constant ≤ 1 μM) could be estimated for the Cu^{I}_{2}-Atx1 dimer. This is consistent with the fact that the absorbance at 304 nm, characteristic of the Cu(I) cluster in the Cu^{I}_{2}-Atx1 dimer, decreases linearly with decreasing protein concentration down to 1.7 μM (data not shown).

The His61Tyr Atx1 variant has also been crystallized in two different arrangements. A side-to-side dimer similar to that in the WT protein (Figure S3b in the Supporting Information) is found for the Cu^{I}_{2} form (rmsd of 0.35 Å for the C^{α} atoms of chain A but 0.71 Å for chain B). The differences are mainly located in α2 and loop 5, the latter being the location of the mutation, and give rise to altered monomer−monomer contacts (contact area ~420 $Å^2$).

Table 2: Equilibrium Constants (K_{ex} Values) for the Exchange of Cu(I) between Atx1 and $PacS_N$ or $CtaA_N$ in 20 mM Hepes, pH 7.0, or 20 mM Taps, pH 8.0, plus 100 mM NaCl

	initial concn (μM)			equilibrium concn (μM)				
proteins (incubation time)	Atx1	$PacS_N$ or $CtaA_N$	Cu	Atx1 total	Cu^I_1-Atx1	$PacS_N$ or $CtaA_N$ total	Cu^I_1-$PacS_N$ or Cu^I_1-$CtaA_N$	K_{ex}
apo-$PacS_N$ + Cu^I_1-Atx1 (5 min, pH 7.0)	50	100	35	44	30	82	5.0	0.03
apo-$PacS_N$ + Cu^I_1-Atx1 (30 min, pH 7.0)	53	53	53	46	38	50	10	0.05
apo-$PacS_N$ + Cu^I_1-Atx1 (30 min, pH 7.0)	10	50	8	10	4.8	44	2.4	0.06
Cu^I_1-$PacS_N$ + apo-Atx1 (5 min, pH 7.0)	60	120	35	52	28	94	3.9	0.04
Cu^I_1-$PacS_N$ + apo-Atx1 (30 min, pH 7.0)	53	53	53	46	39	42	7.4	0.05
apo-$PacS_N$ + Cu^I_2-Atx1 (1.5 min, pH 7.0)	50	50	100	44	61[a]	36	28	5.6
apo-$PacS_N$ + Cu^I_2-Atx1 (30 min, pH 7.0)	50	50	100	47	66[a]	33	26	6.4
Cu^I_1-Atx1 + apo-$CtaA_N$ (5 min, pH 8.0)	40	120	17	37	13	102	1.6	33
apo-Atx1 + Cu^I_1-$CtaA_N$ (5 min, pH 8.0)	34	34	19	30	15	27	1.1	25
apo-Atx1 + Cu^I_1-$CtaA_N$ (5 min, pH 8.0)	30	58	17	28	15	50	2.6	20

[a]The total Cu(I) concentration eluted in the Atx1 fractions. In the transfer from Cu^I_2-Atx1 to apo-$PacS_N$, $PacS_N$ was recovered from two separate fractions (~50% eluted with buffer without added NaCl as fully copper-loaded $PacS_N$, while ~25% eluted with buffer plus 30 mM NaCl as approximately half copper-loaded $PacS_N$). The calculated exchange constants for this experiment are only given for comparison and do not reflect true equilibrium positions.

An almost identical $[Cu_4\{\mu_2\text{-}S^\gamma(Cys)\}_4\{O^\eta(Tyr)\}Cl]^{2-}$ cluster is found (Figure 5b and Figure S3c in the Supporting Information), except that the buried chloride ligand observed in WT Atx1 is replaced by a weakly coordinating phenolate of the introduced Tyr61 of one of the monomers. Consistent with this structure the increase in luminescence upon titrating NaCl into the His61Tyr Cu^I_2-Atx1 dimer (Figure 5d) can be fit to a single site model (eq 2) giving a chloride binding constant of (5.5 ± 0.9) M^{-1} (similar to the value for the external site in the WT protein). For His61Tyr Atx1 quenching of the Tyr61 fluorescence upon the addition of Cu(I) is similar in both the presence and absence of NaCl (Figure 2f), so it is unlikely that Cl^-, even at 200 mM, replaces Tyr as a ligand. These data indicate that a similar side-to-side dimeric arrangement is formed in both the presence and absence of chloride for His61Tyr Cu^I_2-Atx1 and that luminescence increases as a consequence of the binding of this anion. It would therefore appear that the changes observed for the WT Cu^I_2-Atx1 dimer in the presence of chloride are most likely due to the binding of this anion affecting the spectroscopic properties of the Cu^I_4-thiolate cluster and not the overall arrangement of the dimer.

The alternate crystal form for His61Tyr Cu^I_1-Atx1 involves a copper-mediated trimer (two trimers in the asymmetric unit) (Figure S4 in the Supporting Information). His61Tyr Cu^I_1-Atx1 exists primarily as a monomer in solution (Table S3 in the Supporting Information), and therefore this arrangement arises during crystallization. A $[Cu_4\{\mu_3\text{-}S^\gamma(Cys)\}_3\{S^\gamma(Cys)\}_3(H_2O)]^{2-}$ cluster is bound by this trimer (Figure 6a). The three intramolecular copper sites, ligated by Cys12 and Cys15 [bond lengths and angles (139−144°) more consistent with two-coordinate Cu(I)], are almost coplanar with the three S^γ atoms of Cys12 forming a hexameric ring. A significantly longer intermolecular Cu to Cys interaction is present at each of these sites with smaller S−Cu−S angles (101−117°). An additional weakly bound copper ion, which must be acquired during crystallization, is found above the plane of the three core metal ions coordinated by a water molecule (Cu−O distance of ~2.2 Å) and with long bonds to the Cys12 residues from the three monomers. The Cu to Cu distances between this additional copper and the three core coppers are all short (~2.5−2.7 Å).

The binding of Cu(I) by $PacS_N$, PacS95, and $CtaA_N$ results in the appearance of S(Cys) → Cu(I) LMCT bands below 300 nm which increase in intensity up to 1 equiv of copper, after which the protein precipitates (precipitation occurs earlier for PacS95). $CtaA_N$ and $PacS_N$ are both monomeric in the absence and presence of 1 equiv of copper (Table S3 in the Supporting Information). The crystal structure of Cu^I_1-$PacS_N$ has been determined and is the first for the MBD of a copper importer with the native metal bound. A trimeric arrangement is observed through crystallographic symmetry (Figure 6b). The S^γ atoms of Cys14 and Cys17 bind a single copper ion, with the coordination sphere completed by a more weakly interacting Cys14 (S^γ) from a neighboring molecule (Figure 6c). This trimeric arrangement is stabilized during crystallization, as is the case for His61Tyr Cu^I_1-Atx1 and also the CopZ trimer (*30*). Additional electron density above the plane of the three copper ions, in a similar position as the additional copper in the His61Tyr Atx1 trimer, was observed in the Cu^I_1-$PacS_N$ structure but could not be unambiguously assigned (anomalous difference maps confirm this is not copper in this case). Additional density was also observed in a second low-resolution structure of Cu^I_1-$PacS_N$ from a crystal grown in the presence of iodide and could be assigned to this atom. There is a clear possibility for an additional interaction at this position.

The $PacS_N$ and His61Tyr Atx1 trimers are similar and exhibit sizable differences to that of CopZ. All three proteins have a Tyr residue in the second-coordination sphere positioned on loop 5 which hydrogen bonds to a Cys ligand in $PacS_N$ and His61Tyr Atx1 (Cys17 and Cys15, respectively) but not in this arrangement of CopZ (*30*). As well as hydrogen bonding to a coordinating Cys, this Tyr residue hydrogen bonds to a water molecule and makes a weak interaction with the backbone NH of the Ala residue next to the second Cys of the CXXC motif of an adjacent monomer in $PacS_N$ and His61Tyr Atx1 (Ala16 and Ala14, respectively). The CopZ trimer (*30*) is stabilized by hydrogen bonds between the N^ξ of Lys18 of one monomer and the backbone carbonyl of Asp62 of the adjacent chain and also between the $N^{\delta1}$ of His15 on the $C^{13}XXC^{16}$ motif and the backbone carbonyl of Gln63. Tyr65 on loop 5 hydrogen bonds with two water molecules only in the CopZ trimer. The altered trimer arrangement results in changes around the copper site of CopZ compared to $PacS_N$ and His61Tyr Atx1. The backbone amides of Arg13 and Ala16 in $PacS_N$, and Ala11 and Ala14 in His61Tyr Atx1, hydrogen bond to the coordinating thiolates of the Cys ligands. In the CopZ trimer only one of these interactions

is present. In both the $PacS_N$ and His61Tyr Atx1 trimers the more N-terminal Cys ligand provides a long intermolecular interaction at each of the copper sites (intramonomer copper sites in the case of His61Tyr Atx1). In CopZ the more C-terminal Cys ligand provides a short intermonomer Cu−S(Cys16) bond with a lengthening of the intramonomeric Cu−S(Cys16) bond (*30*). The distances between the copper ions are also similar in $PacS_N$ (4.0 Å) and the His61Tyr Atx1 trimer (~4.0−4.2 Å for the intramolecular coppers) but are considerably shorter in the CopZ trimer (3.12 Å). Furthermore, in both $PacS_N$ and His61Tyr Atx1 almost coplanar $Cu_3S^{\gamma}(Cys12/Cys14)_3$ hexameric rings are found (Figure 6a,c) which is not the case in CopZ (*30*).

Copper Transfers. The ability of Cu(I) to pass along the proposed *Synechocystis* copper trafficking pathway from CtaA to Atx1 and onto PacS has been investigated using transfer experiments between partners (Table 2). Typical recoveries from these experiments were 95 ± 10% for Atx1, 85 ± 10% for $PacS_N$ and $CtaA_N$, and 95 ± 10% for copper. Cu(I) exchange is reversible [K_{ex} is the same when starting from Cu^I_1-Atx1 and apo-$PacS_N$ (or apo-$CtaA_N$), as with Cu^I_1-$PacS_N$ (or Cu^I_1-$CtaA_N$) and apo-Atx1], and equilibrium is reached after less than 5 min. The transfer of Cu(I) from $CtaA_N$ to Atx1 is favorable, but only approximately 20% of the copper transfers from the Cu^I_1-Atx1 dimer to $PacS_N$ (Table 2). Copper is readily transferred from the Cu^I_2-Atx1 dimer to $PacS_N$ (Table 2). In the experiments with Cu^I_2-Atx1 ~50% of $PacS_N$ eluted with buffer without added NaCl as fully copper-loaded protein, while ~25% eluted with buffer plus 30 mM NaCl as approximately half copper-loaded $PacS_N$. Relatively low recoveries (~75%) were obtained probably due to the tendency of Cu(I)-$PacS_N$ to precipitate during the experiment. Atx1 was eluted with buffer plus 500 mM NaCl as Cu^I_1-Atx1 plus 40% Cu^I_2-Atx1.

DISCUSSION

A trafficking pathway provides copper to the thylakoid compartments of cyanobacteria for photosynthesis and respiration (Figure 1). This relatively simple pathway is a good model for related, but more complex, human systems where copper mishandling is associated with a range of disorders (*48*, *49*). In this work we show that two different dimeric arrangements of the copper-loaded Atx1 from the *Synechocystis* copper-import pathway can exist in solution at low protein concentrations, and we have determined the crystal structures of these dimers. The head-to-head Cu^I_1-Atx1 dimer will be present in the very low micromolar range under copper-limiting conditions, while the side-to-side Cu^I_2-Atx1 dimer will form more readily if more than 1 equiv of copper is available. It is interesting to note that the physiological concentration of any Atx1 is not known and almost all *in vitro* studies on Atx1s and their interactions have been performed at relatively high protein concentrations. The presence of His61 in the second coordination sphere stabilizes the Cu^I_1-Atx1 head-to-head arrangement. The occurrence of a His residue in this location on loop 5 is unique to certain cyanobacterial Atx1s, supporting a physiological role for this dimer. His61 also gives rise to an additional metal-binding site in this arrangement that can be partially occupied with Cu(I). CopZ also dimerizes in the presence of 1 equiv of Cu(I) (*27*) probably due to the presence of His15, which can also coordinate the metal at a four-copper cluster (*29*). As the formation of the Cu^I_2-Atx1 side-to-side dimer and its Cu^I_4 cluster is only dependent on the availability of copper (and perhaps also chloride) and forms with either a His or Tyr residue at position 61, it could be a more general feature of this family of proteins, particularly under conditions of copper stress.

Copper transfer from $CtaA_N$ to Atx1 is favorable. Copper is readily transferred from dimeric Cu^I_2-Atx1 to $PacS_N$, but transfer from the Cu^I_1 dimer is much less favorable. The dimerization of Atx1 could therefore dictate the subsequent fate of the metal and influence the function of the protein. Metallothioneins are common storage proteins for Cu(I), but bacterial analogues seldom bind Cu(I) (*50*). Cyanobacteria are rare examples of prokaryotes with a cytoplasmic requirement for copper, and a role for Atx1 in recycling endogenous copper has been proposed based on *in vivo* studies which demonstrated that CtaA is not essential for Atx1 function (*12*). Dimerization and copper cluster formation could help to buffer copper under certain conditions. The weaker copper site in the Cu^I_2-Atx1 dimer cannot be loaded by $CtaA_N$ (or $PacS_N$) and is removed by DTT and glutathione. Glutathione could therefore acquire this copper *in vivo* assisting in copper recycling. Dimerization upon copper binding may have additional roles. For example, Hah1 can function as a copper-dependent transcription factor (*51*) that would presumably be aided by sizable copper-induced changes in structure, and dimerization in the presence of metal has been found (*19*, *24*, *31*).

Copper transfer from Atx1 to the MDBs of copper-transporting ATPases, the purported target for the metal [metallochaperones can deliver Cu(I) directly to the transmembrane metal site with a regulatory function proposed for the MBDs (*52*)], involves a copper-dependent side-to-side complex in the examples that have been studied (*46*, *47*). Single-molecule studies of the interaction between Hah1 and the fourth MBD of the Wilson ATPase identified two distinct complexes for the apoproteins (*53*). The head-to-head and side-to-side Atx1 dimers provide models of two different complexes for the interaction of the cyanobacterial metallochaperone with the donating and accepting proteins (both MBDs in this system). If a side-to-side complex is involved in Cu(I) transfer from Atx1 to $PacS_N$ (*17*), then the intermolecular copper site in the side-to-side homodimer provides a model of a potential intermediate. In the structure of His61Tyr Atx1 the introduced phenolate binds to this Cu(I) ion, indicating that Tyr65 of $PacS_N$ could be involved in Cu(I) transfer.

The Atx1 from *Synechocystis* exhibits remarkable Cu(I)-binding flexibility. In addition to the dimeric arrangements observed for the WT protein, a trimer forms for His61Tyr Atx1 possessing a $[Cu_4\{\mu_3\text{-}S^{\gamma}(Cys)\}_3\{S^{\gamma}(Cys)\}_3(H_2O)]^{2-}$ cluster that elicits an additional Cu(I) ion. This is also the case for the cluster formed by the yeast Atx1 trimer in the presence of tetrathiomolybdate (*32*), which has been linked with molybdate-induced copper deficiency via the inhibition of copper trafficking (*32*) and also with the usefulness of tetrathiomolybdate in treating Wilson's disease (*54*, *55*). In all cases, including $PacS_N$ and CopZ (*30*), trimer formation is dominated by metal clusters which possess hexameric Cu_3S_3 rings that are particularly stable and are commonly found in Cu(I)-thiolate complexes (*56*). The trimers of His61Tyr Atx1 and $PacS_N$ are much less stable in solution than the dimeric forms of Atx1 and are favored during crystallization. Aberrant oligomerization and metal cluster formation could be problematic for a cell under certain conditions, including diseased states.

Copper cluster formation has been identified by X-ray absorption spectroscopy in a number of other copper homeostasis and regulatory proteins. This includes Cox17, a copper chaperone for cytochrome *c* oxidase (*57*), the human copper chaperone for Cu,

Zn-superoxide dismutase (*58*), the C-terminal domain of the copper transporter Ctr1 from *S. cerevisiae* (*13*), and the N-terminal domains of the human P-type ATPases (*59*, *60*) as well as the copper-regulated transcription factors Ace1 and Mac1 (*61*, *62*). A number of these are thought to bind four Cu(I) ions via up to six Cys residues in a $[Cu^{I}_{4}\{\mu_2\text{-}S^{\gamma}(Cys)\}_6]^{2-}$ cluster, also possessing hexameric Cu_3S_3 rings, with the metal ions in a tetrahedral arrangement (*13*, *57*, *58*, *61*, *62*). The copper clusters in the side-to-side Atx1 dimers have not previously been observed in biological systems. The $[Cu_4\{\mu_2\text{-}S^{\gamma}(Cys)\}_4]$ core of these structures reveals a Cu^{I}_{4} cluster that can be formed using only four Cys ligands without the presence of Cu_3S_3 rings. As well as providing insight into copper homeostasis, the clusters visualized in this study extend the landscape of potential arrangements that can be used to model spectroscopically derived structures in less well defined systems.

ACKNOWLEDGMENT

We are grateful to Nigel Robinson for DNA encoding CtaA, Atx1, and PacS and for encouraging us to perform these studies using the cyanobacterial system. We thank Brian Keith for performing preliminary studies on $CtaA_N$ and the staff of the ESRF and DLS synchrotron radiation sources and Dr. Arnaud Baslé for assistance with data collection.

SUPPORTING INFORMATION AVAILABLE

Materials and methods and figures showing Cu(I) binding by WT and His61Tyr Atx1, the structures of WT Atx1 head-to-head dimers, WT and His61Tyr side-to-side dimers, and the His61Tyr trimer, and tables showing crystallization conditions, mass analyses, and gel filtration elution volumes. This material is available free of charge via the Internet at http://pubs.acs.org.

REFERENCES

1. Odermatt, A., and Solioz, M. (1995) Two trans-acting metalloregulatory proteins controlling expression of the copper-ATPases of *Enterococcus hirae*. *J. Biol. Chem. 270*, 4349–4354.
2. Pufahl, R. A., Singer, C. P., Peariso, K. L., Lin, S. J., Schmidt, P. J., Fahrni, C. J., Culotta, V. C., Penner-Hahn, J. E., and O'Halloran, T. V. (1997) Metal ion chaperone function of the soluble Cu(I) receptor Atx1. *Science 278*, 853–856.
3. Valentine, J. S., and Gralla, E. B. (1997) Delivering copper inside yeast and human cells. *Science 278*, 817–818.
4. O'Halloran, T. V., and Culotta, V. C. (2000) Metallochaperones, an intracellular shuttle service for metal ions. *J. Biol. Chem. 275*, 25057–25060.
5. Finney, L. A., and O'Halloran, T. V. (2003) Transition metal speciation in the cell: Insights from the chemistry of metal ion receptors. *Science 300*, 931–936.
6. Carr, H. S., and Winge, D. R. (2003) Assembly of cytochrome *c* oxidase within the mitochondrion. *Acc. Chem. Res. 36*, 309–316.
7. Tottey, S., Waldron, K. J., Firbank, S. J., Reale, B., Bessant, C., Sato, K., Cheek, T. R., Gray, J., Banfield, M. J., Dennison, C., and Robinson, N. J. (2008) Protein-folding location can regulate manganese-binding versus copper- or zinc-binding. *Nature 455*, 1138–1142.
8. Macomber, L., and Imlay, J. A. (2009) The iron-sulfur clusters of dehydratases are primary intracellular targets of copper toxicity. *Proc. Natl. Acad. Sci. U.S.A. 106*, 8344–8349.
9. Boal, A. K., and Rosenzweig, A. C. (2009) Structural biology of copper trafficking. *Chem. Rev. 109*, 4760–4779.
10. Robinson, N. J., and Winge, D. R. (2010) Copper metallochaperones. *Annu. Rev. Biochem. 79*, 537–562.
11. Tottey, S., Rich, P. R., Rondet, S. A., and Robinson, N. J. (2001) Two Menkes-type ATPases supply copper for photosynthesis in *Synechocystis* PCC 6803. *J. Biol. Chem. 276*, 19999–20004.
12. Tottey, S., Rondet, S. A., Borrelly, G. P., Robinson, P. J., Rich, P. R., and Robinson, N. J. (2002) A copper metallochaperone for photosynthesis and respiration reveals metal-specific targets, interaction with an importer, and alternative sites for copper acquisition. *J. Biol. Chem. 277*, 5490–5497.
13. Xiao, Z., Loughlin, F., George, G. N., Howlett, G. J., and Wedd, A. G. (2004) C-terminal domain of the membrane copper transporter Ctr1 from *Saccharomyces cerevisiae* binds four Cu(I) ions as a cuprous-thiolate polynuclear cluster: Sub-femtomolar Cu(I) affinity of three proteins involved in copper trafficking. *J. Am. Chem. Soc. 126*, 3081–3090.
14. Zhou, L., Singleton, C., and Le Brun, N. E. (2008) High Cu(I) and low proton affinities of the CXXC motif of *Bacillus subtilis* CopZ. *Biochem. J. 413*, 459–465.
15. Davis, A. V., and O'Halloran, T. V. (2008) A place for thioether chemistry in cellular copper ion recognition and trafficking. *Nat. Chem. Biol. 4*, 148–151.
16. Banci, L., Bertini, I., Ciofi-Baffoni, S., Su, X. C., Borrelly, G. P., and Robinson, N. J. (2004) Solution structures of a cyanobacterial metallochaperone: Insight into an atypical copper-binding motif. *J. Biol. Chem. 279*, 27502–27510.
17. Banci, L., Bertini, I., Ciofi-Baffoni, S., Kandias, N. G., Robinson, N. J., Spyroulias, G. A., Su, X. C., Tottey, S., and Vanarotti, M. (2006) The delivery of copper for thylakoid import observed by NMR. *Proc. Natl. Acad. Sci. U.S.A. 103*, 8320–8325.
18. Borrelly, G. P., Blindauer, C. A., Schmid, R., Butler, C. S., Cooper, C. E., Harvey, I., Sadler, P. J., and Robinson, N. J. (2004) A novel copper site in a cyanobacterial metallochaperone. *Biochem. J. 378*, 293–297.
19. Wernimont, A. K., Huffman, D. L., Lamb, A. L., O'Halloran, T. V., and Rosenzweig, A. C. (2000) Structural basis for copper transfer by the metallochaperone for the Menkes/Wilson disease proteins. *Nat. Struct. Biol. 7*, 766–771.
20. Arnesano, F., Banci, L., Bertini, I., Huffman, D. L., and O'Halloran, T. V. (2001) Solution structure of the Cu(I) and apo forms of the yeast metallochaperone Atx1. *Biochemistry 40*, 1528–1539.
21. Hussain, F., Olson, J. S., and Wittung-Stafshede, P. (2008) Conserved residues modulate copper release in human copper chaperone Atox1. *Proc. Natl. Acad. Sci. U.S.A. 105*, 11158–11163.
22. Hussain, F., Rodriguez-Granillo, A., and Wittung-Stafshede, P. (2009) Lysine-60 in copper chaperone Atox1 plays an essential role in adduct formation with a target Wilson disease domain. *J. Am. Chem. Soc. 131*, 16371–16373.
23. Portnoy, M. E., Rosenzweig, A. C., Rae, T., Huffman, D. L., O'Halloran, T. V., and Culotta, V. C. (1999) Structure-function analyses of the Atx1 metallochaperone. *J. Biol. Chem. 274*, 15041–15045.
24. Tanchou, V., Gas, F., Urvoas, A., Cougouluègne, F., Ruat, S., Averseng, O., and Quéméneur, E. (2004) Copper-mediated homodimerisation for the HAH1 metallochaperone. *Biochem. Biophys. Res. Commun. 325*, 388–394.
25. Miras, R., Morin, I., Jacquin, O., Cuillel, M., Guillain, F., and Mintz, E. (2008) Interplay between glutathione, Atx1 and copper. 1. Copper(I) glutathionate induced dimerization of Atx1. *J. Biol. Inorg. Chem. 13*, 195–205.
26. Poger, D., Fillaux, C., Miras, R., Crouzy, S., Delangle, P., Mintz, E., Den Auwer, C., and Ferrand, M. (2008) Interplay between glutathione, Atx1 and copper: X-ray absorption spectroscopy determination of Cu(I) environment in an Atx1 dimer. *J. Biol. Inorg. Chem. 13*, 1239–1248.
27. Kihlken, M. A., Leech, A. P., and Le Brun, N. E. (2002) Copper-mediated dimerization of CopZ, a predicted copper chaperone from *Bacillus subtilis*. *Biochem. J. 368*, 729–739.
28. Banci, L., Bertini, I., Del Conte, R., Mangani, S., and Meyer-Klaucke, W. (2003) X-ray absorption and NMR spectroscopic studies of CopZ, a copper chaperone in *Bacillus subtilis*: The coordination properties of the copper ion. *Biochemistry 42*, 2467–2474.
29. Hearnshaw, S., West, C., Singleton, C., Zhou, L., Kihlken, M. A., Strange, R. W., Le Brun, N. E., and Hemmings, A. M. (2009) A tetranuclear Cu(I) cluster in the metallochaperone protein CopZ. *Biochemistry 48*, 9324–9326.
30. Singleton, C., Hearnshaw, S., Zhou, L., Le Brun, N. E., and Hemmings, A. M. (2009) Mechanistic insights into Cu(I) cluster transfer between the chaperone CopZ and its cognate Cu(I)-transporting P-type ATPase, CopA. *Biochem. J. 424*, 347–356.
31. Boal, A. K., and Rosenzweig, A. C. (2009) Crystal structures of cisplatin bound to a human copper chaperone. *J. Am. Chem. Soc. 131*, 14196–14197.
32. Alvarez, H. M., Xue, Y., Robinson, C. D., Canalizo-Hernández, M. A., Marvin, R. G., Kelly, R. A., Mondragón, A., Penner-Hahn, J. E., and O'Halloran, T. V. (2009) Tetrathiomolybdate inhibits copper trafficking proteins through metal cluster formation. *Science 327*, 331–334.

33. Diederix, R. E. M., Canters, G. W., and Dennison, C. (2000) The Met99Gln mutant of amicyanin from *Paracoccus versutus*. *Biochemistry 39*, 9551–9560.
34. Ellman, G. L. (1959) Tissue sulfhydryl groups. *Arch. Biochem. Biophys. 82*, 70–77.
35. Gill, S. C., and von Hippel, P. H. (1989) Calculation of protein extinction coefficients from amino acid sequence data. *Anal. Biochem. 182*, 319–326.
36. Woodbury, R. L., Hardy, S. J. S., and Randall, L. L. (2002) Complex behavior in solution of homodimeric SecA. *Protein Sci. 11*, 875–882.
37. Leslie, A. G. (2006) The integration of macromolecular diffraction data. *Acta Crystallogr., Sect. D: Biol. Crystallogr. 62*, 48–57.
38. Collaborative Computational Project Number 4 (1994) The CCP4 suite: Programs for protein crystallography. *Acta Crystallogr., Sect. D: Biol. Crystallogr. 50*, 760–763.
39. Morris, R. J., Perrakis, A., and Lamzin, V. S. (2003) ARP/wARP and automatic interpretation of protein electron density maps. *Methods Enzymol. 374*, 229–244.
40. Emsley, P., and Cowtan, K. (2004) Coot: Model-building tools for molecular graphics. *Acta Crystallogr., Sect. D: Biol. Crystallogr. 60*, 2126–2132.
41. Sheldrick, G. M. (2008) A short history of SHELX. *Acta Crystallogr. A 64*, 112–122.
42. Adams, P. D., Grosse-Kunstleve, R. W., Hung, L. W., Ioerger, T. R., McCoy, A. J., Moriarty, N. W., Read, R. J., Sacchettini, J. C., Sauter, N. K., and Terwilliger, T. C. (2002) PHENIX: Building new software for automated crystallographic structure determination. *Acta Crystallogr., Sect. D: Biol. Crystallogr. 58*, 1948–1954.
43. Davis, I. W., Leaver-Fay, A., Chen, V. B., Block, J. N., Kapral, G. J., Wang, X., Murray, L. W., Arendall, W. B., Snoeyink, J., Richardson, J. S., and Richardson, D. C. (2007) MolProbity: All-atom contacts and structure validation for proteins and nucleic acids. *Nucleic Acids Res. 35*, W375–383.
44. Kleywegt, G. J., Zou, J. Y., Kjeldgaard, M., and Jones, T. A. (2001) International Tables for Crystallography, Vol. F. Crystallography of Biological Macromolecules (Rossmann MGaA, E., Ed.) Kluwer Academic, Dordrecht, The Netherlands.
45. Krissinel, E., and Henrick, K. (2007) Inference of macromolecular assemblies from crystalline state. *J. Mol. Biol. 372*, 774–797.
46. Banci, L., Bertini, I., Cantini, F., Felli, I. C., Gonnelli, L., Hadjiliadis, N., Pierattelli, R., Rosato, A., and Voulgaris, P. (2006) The Atx1-Ccc2 complex is a metal-mediated protein-protein interaction. *Nat. Chem. Biol. 2*, 367–368.
47. Banci, L., Bertini, I., Calderone, V., Della-Malva, N., Felli, I. C., Neri, S., Pavelkova, A., and Rosato, A. (2009) Copper(I)-mediated protein-protein interactions result from suboptimal interaction surfaces. *Biochem. J. 422*, 37–42.
48. Bush, A. I. (2000) Metals and neuroscience. *Curr. Opin. Chem. Biol. 4*, 184–191.
49. Madsen., E., and Gitlin, J. D. (2007) Copper and iron disorders of the brain. *Annu. Rev. Neurosci. 30*, 317–337.
50. Gold, B., Deng, H., Bryk, R., Vargas, D., Eliezer, D., Roberts, J., Jiang, X., and Nathan, C. (2008) Identification of a copper-binding metallothionein in pathogenic mycobacteria. *Nat. Chem. Biol. 4*, 609–616.
51. Itoh, S., Kim, H. W., Nakagawa, O., Ozumi, K., Lessner, S. M., Aoki, H., Akram, K., McKinney, R. D., Ushio-Fukai, M., and Fukai, T. (2008) Novel role of antioxidant-1 (Atox1) as a copper-dependent transcription factor involved in cell proliferation. *J. Biol. Chem. 283*, 9157–9167.
52. González-Guerrero, M., and Argüello, J. M. (2008) Mechanism of Cu^+-transporting ATPases: Soluble Cu^+ chaperones directly transfer Cu^+ to transmembrane transport sites. *Proc. Natl. Acad. Sci. U.S.A. 105*, 5992–5997.
53. Benítez, J. J., Keller, A. M., Ochieng, P., Yatsunyk, L. A., Huffman, D. L., Rosenzweig, A. C., and Chen, P. (2008) Probing transient copper-chaperone-Wilson disease protein interactions at the single-molecule level with nanovesicle trapping. *J. Am. Chem. Soc. 130*, 2446–2447.
54. George, G. N., Pickering, I. J., Harris, H. H., Gailer, J., Klein, D., Lichtmannegger, J., and Summer, K. H. (2003) Tetrathiomolybdate causes formation of hepatic copper-molybdenum clusters in an animal model of Wilson's disease. *J. Am. Chem. Soc. 125*, 1704–1705.
55. Zhang, L., Lichtmannegger, J., Summer, K. H., Webb, S., Pickering, I. J., and George, G. N. (2009) Tracing copper-thiomolybdate complexes in a prospective treatment for Wilson's disease. *Biochemistry 48*, 891–897.
56. Blackburn, N. J. (2010) A tale of two metals. *Chem. Biol. 17*, 8–9.
57. Heaton, D. N., George, G. N., Garrison, G., and Winge, D. R. (2001) The mitochondrial copper metallochaperone Cox17 exists as an oligomeric, polycopper complex. *Biochemistry 40*, 743–751.
58. Strasser, J. P., Siluvai, G. S., Barry, A. N., and Blackburn, N. J. (2007) A multinuclear copper(I) cluster forms the dimerization interface in copper-loaded human copper chaperone for superoxide dismutase. *Biochemistry 46*, 11845–11856.
59. Cobine, P. A., George, G. N., Winzor, D. J., Harrison, M. D., Mogahaddas, S., and Dameron, C. T. (2000) Stoichiometry of complex formation between copper(I) and the N-terminal domain of the Menkes protein. *Biochemistry 39*, 6857–6863.
60. Ralle, M., Lutsenko, S., and Blackburn, N. J. (2004) Copper transfer to the N-terminal domain of the Wilson disease protein (ATP7B): X-ray absorption spectroscopy of reconstituted and chaperone-loaded metal binding domains and their interaction with exogenous ligands. *J. Inorg. Biochem. 98*, 765–774.
61. Pickering, I. J., George, G. N., Dameron, C. T., Kurz, B., Winge, D. R., and Dance, I. G. (1993) X-ray absorption spectroscopy of cuprous-thiolate clusters in proteins and model systems. *J. Am. Chem. Soc. 115*, 9498–9505.
62. Brown, K. R., Keller, G. L., Pickering, I. J., Harris, H. H., George, G. N., and Winge, D. R. (2002) Structures of the cuprous-thiolate clusters of the Mac1 and Ace1 transcriptional activators. *Biochemistry 41*, 6469–6476.